Fabrication of thermal-based vacuum gauge

Ho Jung, Tae Hyun Kim, Kyung Tae Kim, Jae Hong Park, Hee Yeoun Kim

National Nano Fab Center, 335 Gwahangro Yuseong-gu, Daejeon, Republic of Korea
E-mail: hyeounkim@nnfc.re.kr

Published in Micro & Nano Letters; Received on 29th June 2014; Revised on 23rd October 2014; Accepted on 30th October 2014

The fabrication and evaluation of a wide-range vacuum gauge for monitoring the pressure level inside an infrared focal plane array and a wafer-level packaging (WLP) are reported. The proposed vacuum gauge has a microbolometer structure produced using the conventional surface micromachining process to achieve thermal isolation and high sensitivity. This structure has other advantages such as fast response time, a wider measurement range and easier integration to a Si substrate compared with other pressure sensors. The evaluation results show that the fabricated vacuum gauge has a linear dynamic range and a sensitivity of 10^{-3} to 10^{5} K/W/torr for vacuum pressures ranging from 10^{-6} to 760 torr. Also, the response time to vacuum change is reduced from 0.11 s at 10^{-5} torr to 15 ms at 100 torr. Therefore, the microbolometer-based vacuum gauge has good potential for application in WLP, and it is possible to hermetically seal it with various read-out integrated circuit substrates.

1. Introduction: Since the development of the Pirani gauge in the early 1900s, many gauges have been developed for measuring pressure in the range of 10^{-5} to 1000 torr [1–4]. Among these, the micro Pirani gauge can easily measure the pressure levels inside a hermetically sealed packaging, and it is fabricated using a simple process. Compared with other mechanisms for pressure detection in microstructures, such as the Q-factor, resonance and helium leak test, the Pirani gauge has the advantages of low cost, high sensitivity and effective integration. However, it has some disadvantages, such as high thermal loss, narrow dynamic range, external shock waves and short life because the sensors consist primarily of wires, ladders and membranes [5–8].

To overcome these drawbacks, a vacuum gauge with better performance and wider dynamic range compared with conventional sensors is needed. A microbolometer-based vacuum gauge has many advantages, such as faster response time, smaller size and higher sensitivity, over conventional MEMS gauges. Furthermore, a microbolometer-based vacuum gauge does not need an additional chip fabricated by a different process for pressure monitoring because the microbolometer pixel itself can be used as a temperature sensor, IR sensor and vacuum gauge [9].

In this Letter we discuss the characteristics of the microbolometer-based vacuum gauge fabricated by the same method used for an IR detector. The gauge is also integrated and measured with the read-out integrated circuit substrate. Finally, we assess its application in vacuum measurement and its long-term stability in wafer-level packaging (WLP).

2. Design: The microbolometer-based vacuum gauge is fabricated using conventional surface micromachining technology with a thermally isolated structure. Fig. 1 shows a schematic of the proposed device. The vacuum gauge consists of two parts – a highly sensitive membrane and a micro-machined floating structure. The operation of the vacuum gauge designed here is identical to a conventional vacuum gauge.

To verify the thermal property of the structure, thermal simulation was performed using a CoventorWare simulator, as shown in Fig. 2. In the simulation, by applying a bias ranging from 0 to 1 V in a metal pad, the change in solid thermal conductance per leg length was estimated and optimised. According to the heat balance equation, the power input to the vacuum gauge is equal to the heat lost by the heater to the surroundings. Solid conduction (G_s), gas conduction (G_g) and radiation (G_r) mechanisms contribute to the total heat transfer. Each parameter depends on the isolation structure, leg length and membrane area. To determine the pressure level, first, the radiation mechanism is derived as [10]

$$G_r = 2\varepsilon\sigma A_s(T^2 + T_a^2) + (T + T_a) \tag{1}$$

Here, σ is the Stephen-Boltzmann constant, ε it the emissivity, T and T_a are the temperatures of the floating membrane and ambient, respectively, and A_s is the gauge active area. The second mechanism of gas conduction can be expressed as [11]

$$\begin{aligned} G_g &= \frac{\varphi}{2-\varphi} G_a A_s P\left(\frac{P_{t1}}{P+P_{t1}} + \frac{P_{t2}}{P+P_{t2}}\right) \\ G_a &= \Lambda_0\left(\frac{273.2}{T_a}\right)^{1/2} \end{aligned} \tag{2}$$

Here, φ is the accommodation coefficient of gas; G_a and Λ_0 are the free molecular conductivities at T_a and 273 K, respectively; A_s is the floating membrane area; P is the gas pressure; and P_{t1} and P_{t2} are, respectively, the transition pressures on the lower and upper sides of the floating membrane, which are inversely proportional to the effective separation between the membrane and the heat sinks.

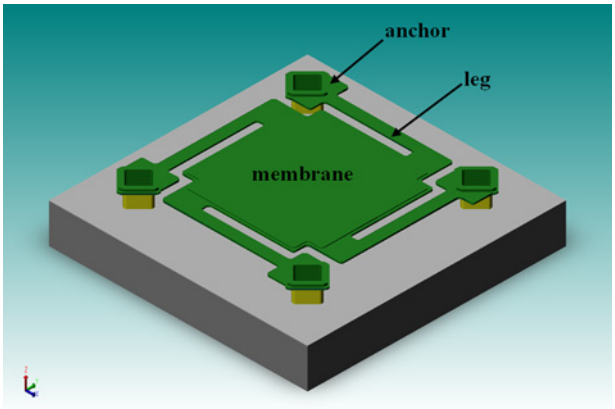


Figure 1 *Schematic structure of the proposed vacuum gauge*

© The Institution of Engineering and Technology 2014

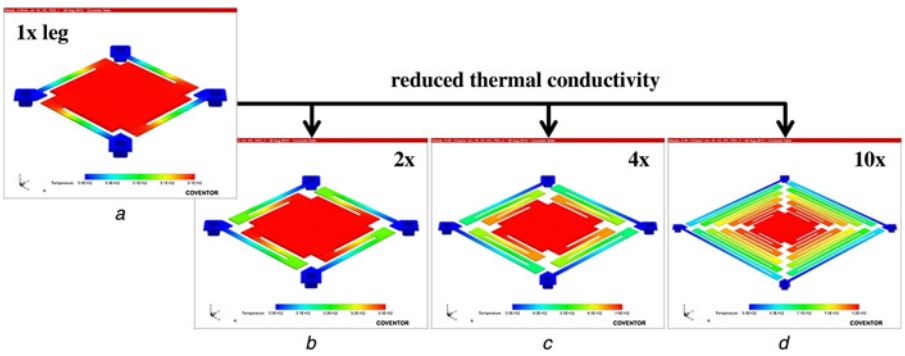


Figure 2 *Simulation results of thermal isolation structure against the vacuum gauge geometry (leg length split)*
a 25 μm(1×)
b 50 μm(2×)
c 100 μm(4×)
d 250 μm(10×)

Third, the mechanism of solid conduction is derived as [11]

$$G_s = \left[\frac{1}{4.2kd}\left(\frac{B}{A}\right) + 5 \times 10^4\right]^{-1} \quad (3)$$

Here, k is the thermal conductivity, and d is the effective thickness of the leads and the spreading resistance close to the lead ends. Fig. 3 shows the numerical simulation of the vacuum gauge using the heat balance theory [12]. Using (1)–(3), the total thermal conductance is calculated as follows: Λ_0 is 0.079 W/cm^2°C, and the parameters φ, P_{t1} and P_{t2} are 0.9, 30 and 0.3, respectively [12]. When the pressure is close to 100 torr, the value of G_g is approximately several tens of times that of G_s, and it is linearly saturated. Moreover, each transition pressure is determined with 10^{-3} torr as the low-pressure point and 100 torr as the high-pressure point. Numerical geometry design and simulation processes were carried out to obtain better performance. As a result, the experimental results of the vacuum gauge closely match the calculated numerical curve. As fewer atoms exist in a gas at lower pressures and the mean free path of the atom is much longer than the distance between the atoms, heat is mostly absorbed by collision with the floating membrane.

Therefore, the pressure is less sensitive to membrane area and more sensitive to the isolation structure of the leg support. To verify the characteristics of the isolation structure at low pressure, various geometric designs were simulated. Fig. 4 shows the results of the simulation for isolation structure lengths of 25 μm (L1X), 50 μm (L2X), 100 μm (L4X) and 250 μm (L10X); width of 1 μm; and gap of 2.3 μm. The simulation predicted that L10X has higher sensitivity at lower pressures, resulting in a wider dynamic range of operation. Therefore, a short and narrow leg structure was used in the design for reducing thermal loss.

3. Fabrication: Fig. 5 shows a schematic of the fabrication process for the proposed MEMS-based vacuum gauge. The fabricated wafer in the vacuum gauge is of 720 μm thickness and of 8 inch diameter. First, a 3000 Å PECVD oxide layer was deposited as an electrical passivation layer. A pad metal (Ti/Al/Ti/TiN) layer was then deposited by the PVD method and patterned by dry etching. For uniformity wafer morphology, a 1.4 μm-thick oxide film layer was deposited and etched by a chemical mechanical polishing process with a three-step standard process. Also, an added etch back process was applied to obtain an improved flat surface. Then, a very thin oxide layer with 100 Å of thickness and 2 μm-thick non-photosensitive material was used as a sacrificial layer to form the gap distance. To improve the conventional stiction and deformation phenomenon, this process was introduced for easy dry-release with a amorphous sacrificial layer which was compatible with the CMOS process. Then, the membrane layer was deposited with a 2000 Å-thick SiNx layer. For the anchor structure, a via etch process was performed in a careful condition because the sacrificial layer diffuses to the lateral direction during the plasma etching period. Next, a 1500 Å-thick TiN layer was deposited and patterned by dry etching in order to be connected from the bottom pad electrode to

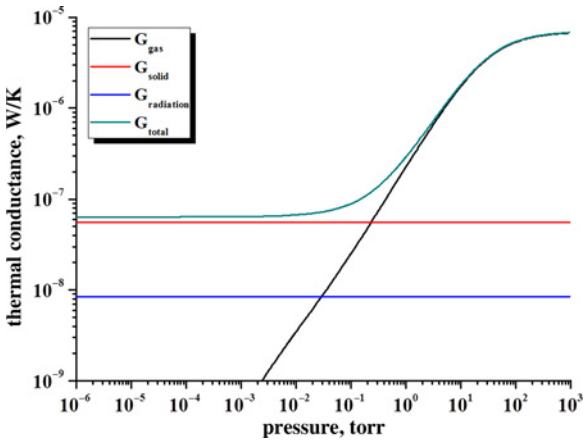


Figure 3 *Numerical modelling as a function of the total conductance with proposed device parameter*

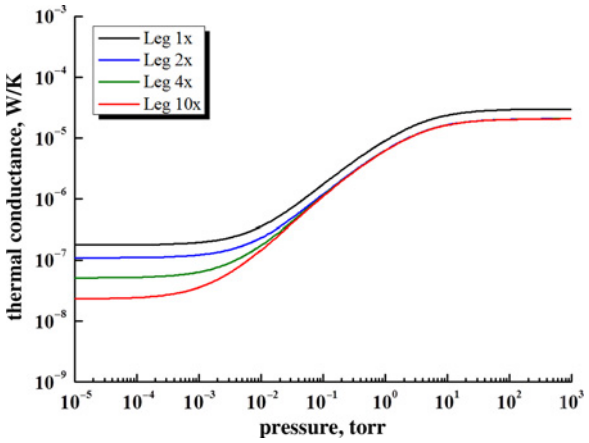


Figure 4 *Numerical simulation as a function of the leg length split with proposed device parameter*

© The Institution of Engineering and Technology 2014

doi: 10.1049/mnl.2014.0378

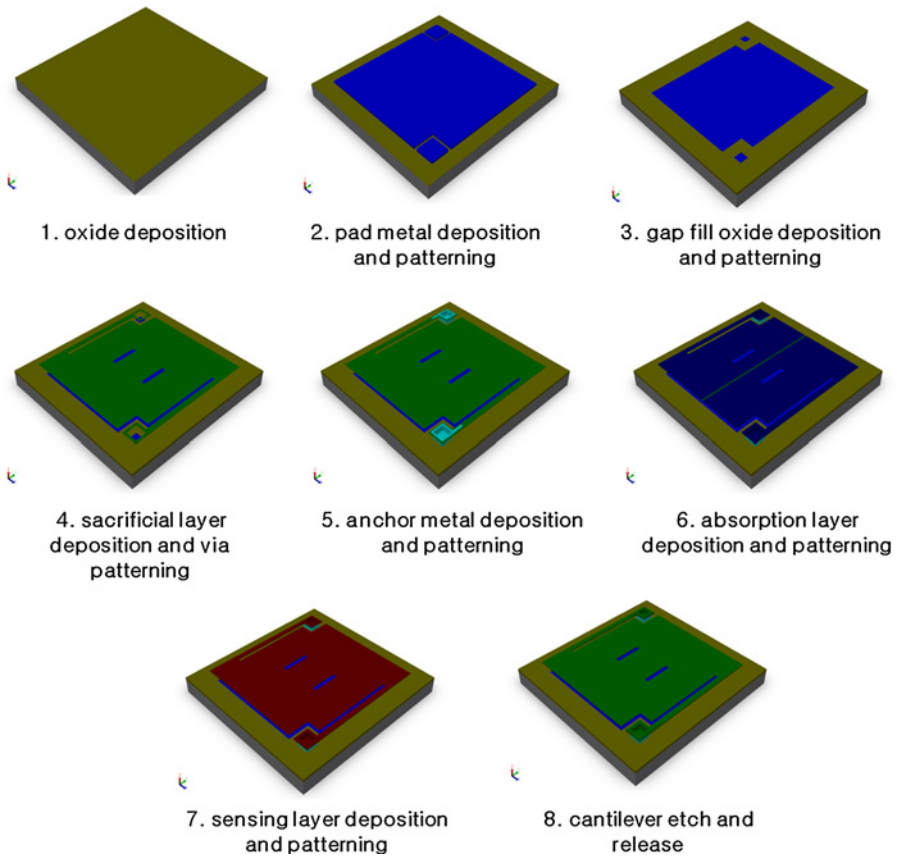


Figure 5 *Process sequence flow of the proposed vacuum gauge*

the anchor. Then, a Ti absorption layer and a 1000 Å-thick amorphous Si layer were deposited as a sensing material, and then they were patterned by dry etching. A top SiNx layer passivation layer with 2000 Å of thickness was deposited and patterned. Finally, the proposed device structure was released by oxygen ashing for 5 to 10 min, see Fig. 6.

Previously, vacuum gauges were fabricated by MEMS technology using polyimide material and bulk micromachining. However, a polyimide layer has drawbacks, such as the fine removal of residual polymer. In addition, conventional MEMS technology with wet etching and a lift-off process can cause serious yield problems, including membrane stiction and deformation. To overcome these problems, we developed a superior dry etching process compatible with the CMOS process. Moreover, it is a low-cost and on-chip process as the gauge is fabricated with the same process as the IR sensor to monitor the pressure level inside the packaging in real time. WLP is a promising three-dimensional (3D) packaging technology for achieving low cost and a small size chip for the microbolometer and it is readily available to the market. However, determining hermeticity inside WLP is difficult. The most conventional test methods for pressure monitoring are membrane deflection, cumulative helium leak detection, the Pirani gauge and the quality factor test. Among these methods, Pirani gauges have been widely used to measure the pressure level in vacuum circumstances and have the advantages of low power, small size, fast response time and a wide operating range. However, as Pirani gauges have a large size for applying the WLP structure, we fabricated a new vacuum gauge for monitoring the vacuum characteristic, reliability inside the WLP structure for the purpose of evaluating the vacuum level of microbolometer, gyroscope, accelerometer and so on (Fig. 7).

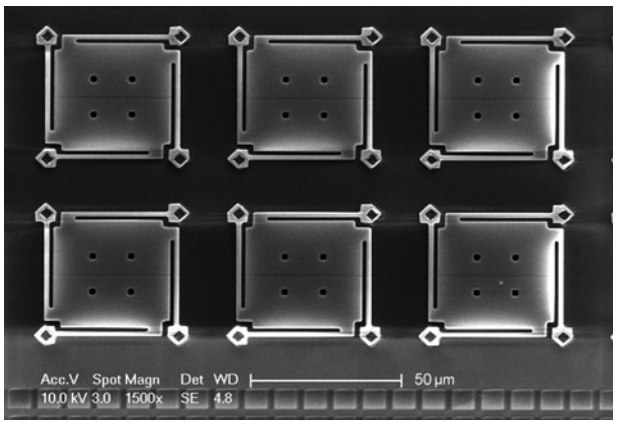


Figure 6 *SEM image of the proposed vacuum gauge*

4. Results and discussion: The response characteristics of the microbolometer-based vacuum gauge were measured using the setup shown in Fig. 8. The device was kept inside a vacuum chamber with a 4-point probe and was tested with a semiconductor parameter analyser to measure the pressure-dependent resistance. Vacuum pressure was obtained using a general rotary pump along with a DH Co. turbo pump with which it was possible to obtain a vacuum state of under 10^{-6} torr.

The flatness of the floated membrane is a very critical parameter in the bolometer and pressure sensor surface. Fig. 6 shows a 3D surface the profile of the fabricated vacuum gauge with an 8×6 µm sensor array and was measured by the Zygo 3D surface profiler. The y-axis shows the flatness deviation of height from the bottom, whereas the x-axis is scanned at the horizontal distance. The measurement result shows that the released plate is not deflected and is maintained uniformly by the anchor structure. Also, the surface

© The Institution of Engineering and Technology 2014

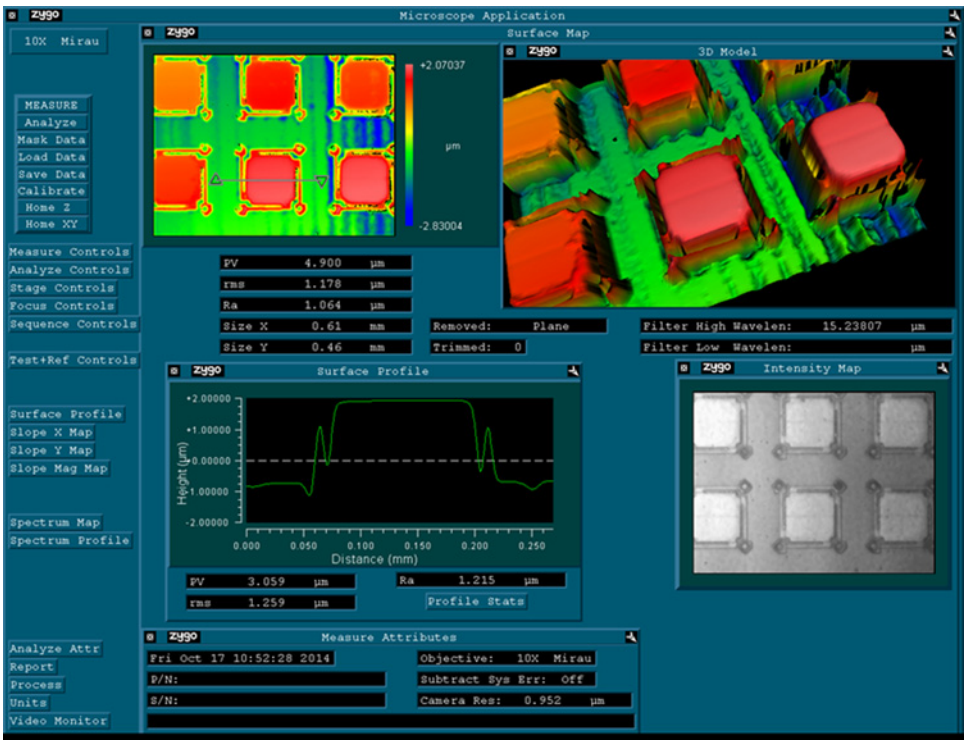


Figure 7 *3D profile analysis of surface flatness of the proposed vacuum gauge*

deviation of the membrane was measured from 40 to 110 nm roughness with a nine edge point of the wafer.

The change in resistance as a function of pressure plays an important role in the determination of sensitivity and dynamic range, which are strongly dependent on the thermal resistance of the gauge material. This change in thermal resistance is proportional to the difference between the resistor values. To increase the performance, the vacuum gauge needs to be carefully designed and fabricated with a larger leg length, a greater membrane area and a smaller gap. A measurement method using the resistance change of the vacuum gauge is also introduced. Fig. 9 shows the resistance curve as a function of the low and high voltage of the vacuum gauge with respect to leg length in the vacuum probe station. Joule heating at low bias voltage is too small to affect the resistance change. The reference value for low voltage is fixed at 0.1 V through repeated resistance measurement. However, resistance at high voltages is affected by Joule heating, which increases with bias voltage. An appropriate high voltage of 0.7 V was determined by varying the input voltage from 0.2 to 1 V in a breakdown test of the device through in-situ monitoring of the vacuum gauge morphology. In the breakdown test, the gauge was destroyed by leg deformation for a bias greater than 0.7 V. The normalised pressure–resistance calibration curve obtained using the low and high voltage method is shown in Fig. 9. To verify the relationship between the rate of change in resistance and total thermal conductance, the temperature increase ΔT was determined from the resistance value of the Si thin film,



Figure 8 *Measurement setup of the proposed vacuum gauge*

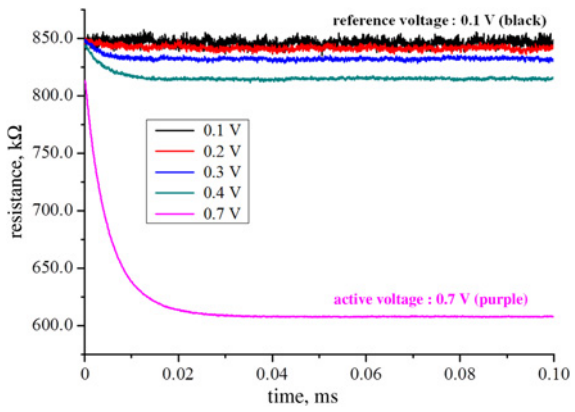


Figure 9 *Resistance curve as a function of low and high voltage of fabricated vacuum gauge*

© The Institution of Engineering and Technology 2014

doi: 10.1049/mnl.2014.0378

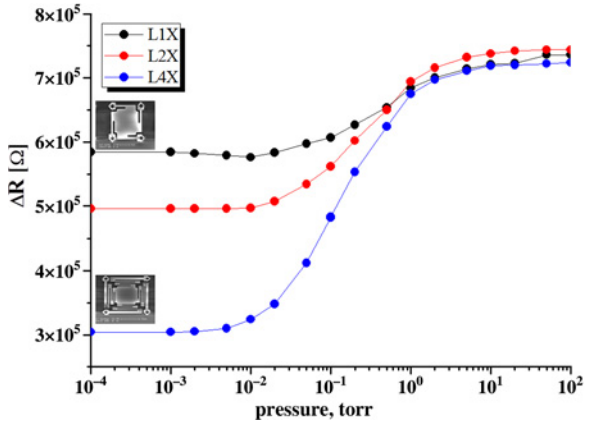


Figure 10 *Resistance change as a function of pressure for proposed vacuum gauge with split of leg length*

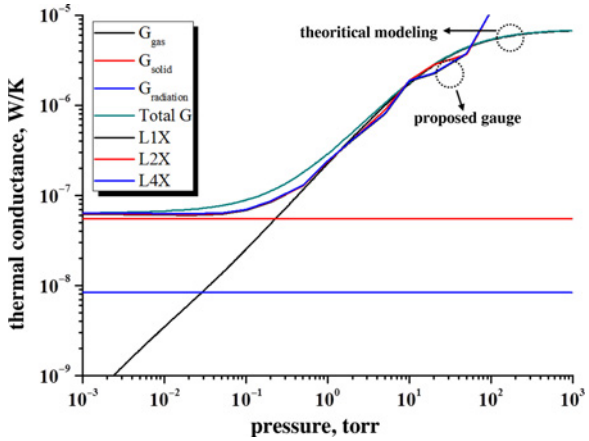


Figure 12 *Experimental result which is fitted to the numerical calculation model to verify conformity of measurement value*

which is [1]

$$R_s = R_a\left[1 + \alpha_a(T - T_a)\right] \tag{4}$$

Here, R_s is the resistance and α_a is the temperature coefficient of the resistance of the active layer at temperature T_a. The results match the resistance change obtained in the numerical calculation. The experimental data for thermal conductance as a function of pressure is shown in Fig. 10.

Fig. 10 also shows the change in resistance as a function of pressure for leg lengths L1X, L2X and L4X in the range 10^{-4} to 100 torr. The measurement results show that the resistance against pressure change curves for the four leg lengths are sigmoid and operate in different pressure zones, illustrating that the vacuum gauge can be used particularly for detecting pressure levels under 10^{-3} torr, which is related to the thermal conductance and the length and width of the a-Si/Si_3N_4 lead. Fig. 11 shows the thermal conductance as a function of pressure for the proposed vacuum gauge. The result indicates that the vacuum gauge can be used to measure pressures ranging from 10^{-3} torr to 10 torr with high sensitivity. However, at pressures below 10^{-3} torr, the sensitivity of the gauge decreased. Hence, to detect ultra-low vacuum pressures, additional process revision was performed with simulation and parameter tuning. Finally, Fig. 12 shows the experimental result matched with the numerical calculation to verify the conformity of the measured values. We derived from 10^{-6} to 1000 torr numerical calculation (green line; G_{total}) of the fabricated device according to the equations which include the proposed device material value of the G_s, G_g and G_r parameters. We also evaluated the total conductance experimentally according to the relationship of the equation $G(T - T_a) = V^2/R_s = IV$, where T_a is the ambient temperature, V^2/R_s is the electrical bias power on the sensor R_s and V is the corresponding voltage drop. Temperature rise $T - T_a$ (ΔR) and TCR was measured from the resistance value of the sensor amorphous film at 0.7 V bias voltage. Finally, the measured data was converted to total thermal conductance per pressure level and fitted to the numerical modelling graph. The tolerance of the theoretical model and the measured value was within 5%. Moreover, the trend seems uniform in a whole pressure region. Therefore, the proposed vacuum gauge can be applied for monitoring the pressure level inside a package device.

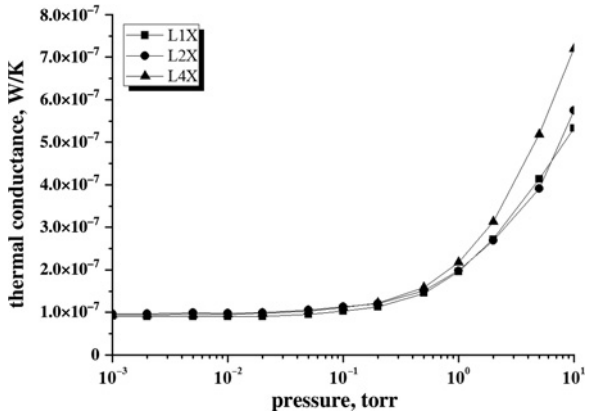


Figure 11 *Thermal conductance as a function of pressure for proposed vacuum gauge*

5. Conclusions: A microbolometer-based vacuum gauge has been designed and fabricated after simulation and theoretical modelling in order to achieve a thermally isolated structure and high sensitivity. To obtain a wide dynamic range and high sensitivity, the leg length and membrane area of the gauge are tuned based on numerical calculations. It is encapsulated in a ceramic package to avoid external interference. Experimental results show that the fabricated vacuum gauge has a wider dynamic range as well as higher sensitivity to measure pressures ranging from 10^{-6} to 760 torr. It also provides linear real-time monitoring. In addition, a preliminary study of the WLP using the vacuum gauge was performed. Hereafter, we will be precisely estimating vacuum characteristics and long-term stability inside the WLP.

6. Acknowledgments: This work was supported by the Daegu Technology Business Program (ACC-2013-DGI-00557) funded by the Ministry of Science, ICT and Future Planning. It was also supported by the Basic Science Research Program through the National Research Foundation of Korea (NRF) funded by the Ministry of Education, Science and Technology (grant no. 2012R1A1A2007707). It was also supported by the Nano Material Technology Development Program through the National Research Foundation of Korea (NRF) funded by the Ministry of Science, ICT and Future Planning (grant no. 2012M3A7B5049567).

7 References

[1] Zhang F.T.: 'A micro-Pirani vacuum gauge based on micro-hotplate technology', *Sensor Actuat A, Phys.*, 2006, **126**, pp. 300–305

© The Institution of Engineering and Technology 2014

[2] Wang X.: 'A micro-machined Pirani gauge for vacuum measurement of ultra-small sized vacuum packaging', *Sensor Actuat A, Phys.*, 2010, **161**, pp. 108–113
[3] Jiang W.: 'A single crystal silicon micro-Pirani vacuum gauge with high aspect ratio structure', *Sensor Actuat A, Phys.*, 2010, **163**, pp. 159–163
[4] Topalli E.S.: 'Pirani vacuum gauges using silicon-on-glass and dissolved-wafer processes for the characterization of MEMS vacuum packaging', *IEEE Sens. J.*, 2009, **9**, pp. 263–270
[5] Purahmad M., Huang J., Plakhotnyuk M.: 'A MEMS-based resistive vacuum gauge with voltage readout'. 26th Int. Vacuum Nanoelectronics Conf., Roanoke, VA, USA, 2013, pp. 8–12
[6] Zaker E.: 'Thermal-based MEMS vacuum gauges for measuring pressures from 10^{-2} Torr to 10^{-6} Torr'. 25th Int. Vacuum Nanoelectronics Conf., Jeju, Korea, 2012, pp. 1–2
[7] Dams F., Schreiner R.: 'A high thermal resistance MEMS-based Pirani vacuum sensor chip'. Smart Sensors, Actuators, and MEMS VI, Grenoble, France, 2013, *Proc. SPIE*, **8763**, p. 87630P
[8] Xiao S., Dehui X., Bin X., Yuelin W.: 'Integrated thermopile vacuum gauge with an XeF_2 dry-etching process', *J. Nanoeng. Nanosyst.*, 2014, **228**, pp. 154–158
[9] Macro M.S.: 'Pressure sensing in vacuum hermetic micropackaging for MOEMS-MEMS', *J. Micro/Nanolith. MEMS MOEMS*, 2010, **9**, pp. 041109-01–041109-10
[10] Shie J.S.: 'High performance Pirani vacuum gauge', *J. Vac. Sci. Technol. A.*, 1995, **13**, pp. 2972–2979
[11] Weng P.K.: 'Micro-Pirani vacuum gauge', *Rev. Sci. Instrum.*, 1993, **65**, pp. 492–499
[12] Chae J.S.: 'A micromachined pirani gauge with dual heat sinks', *IEEE Rans Adv. Pack*, 2005, **28**, pp. 619–625

© The Institution of Engineering and Technology 2014

doi: 10.1049/mnl.2014.0378